Geometry Optimization and Conformational Analysis of $(C_{60})_N$ Clusters Using a Dynamic Lattice-Searching Method

Longjiu Cheng, Wensheng Cai, and Xueguang Shao*[a]

A newly developed unbiased global optimization method, named dynamic lattice searching (DLS), is used to locate putative global minima for all $(C_{60})_N$ clusters with Girifalco potential up to N = 150. A simple greedy strategy is adopted for the basic frame, so DLS has a very high convergence speed and may converge at various configurations. As most structures are packed by basic tetrahedra, some sequences are defined by both configurations and the size of the basic tetrahedra. A sequence-based conformational analysis is carried out with the defined sequences by counting the hit number over 10000 independent DLS runs for all the cases up to N = 150. It was found that the hit rate of a sequence is related to the size of the basic tetrahedra. Use of this method proved that the Leary tetrahedral sequence is dominant in a certain range of cluster sizes, although the sequence has no potential energy advantage. The calculation results are also consistent with those of annealing experiments at high temperature, both in magic numbers and height of the peaks in the mass spectrum.

1. Introduction

The condensed-phase properties of $(C_{60})_N$ molecular clusters have attracted much interest among chemical physics scientists because of their unusual intermolecular potential.[1] It is well-known that the molecules can rotate freely at high temperature, so they act as large pseudo atoms with extremely short-range interactions. The theoretical predictions show that the stable liquid phase of $(C_{60})_N$ molecular clusters only exists over a very narrow temperature range or not at all.[1–4]

Mass spectroscopy experiments on positively charged $(C_{60})_N$ clusters indicated that, similar to Lennard-Jones (LJ) clusters, fullerene clusters favor icosahedral structures.[5] Further experiments on both neutral and charged $(C_{60})_N$ clusters showed similar results, but magic numbers with decahedral packing or close packing are more favored at higher temperature.[6,7] However, theoretical calculations using various potentials contradicted the experimental results.[8–12] For example, calculations using the isotropic Girifalco potential[13] found that icosahedral structures are only lowest in energy up to $N = 13$.[8,11] Above this size, the structures are either decahedral or close-packed. Similar results are obtained using the all-atom potential[14] or the Pacheco and Prates-Ramalho (PPR) potential,[15] where icosahedral structures are lowest in potential energy to a slightly larger size ($N = 15$, 16) than that for the Girifalco potential.[9,10,12]

To explain the difference between experimental results and theoretical calculations, some molecular dynamics (MD) simulations with thermal information were carried out to study the solid–solid transitions in a variety of systems.[10,16–20] However, for all these examples, icosahedral structures are more favored at high temperature. The behavior of these solid–solid transitions is opposite to that found in the experiments. The reason may be that icosahedra have a larger vibrational entropy.[19] Furthermore, a study of the growth of $(C_{60})_N$ clusters shows that there is kinetic trapping for icosahedra.[21] Analysis of the potential energy surface (PES) topography of those LJ clusters with nonicosahedral global minima has shown that large energy barriers exist for interconversion of the icosahedral isomers and the global minima, and the icosahedral funnel is much wider.[22]

The short range of the potential means that the funnels on the PES of the $(C_{60})_N$ pair potential are much deeper than those of the LJ potential, and the local minimization (LM) for $(C_{60})_N$ is much more time-consuming. This property makes unbiased global optimization of $(C_{60})_N$ clusters much more difficult than that of LJ clusters. In recent years, some global optimization methods have been applied to $(C_{60})_N$ clusters,[10–12] such as genetic algorithm (GA), fast annealing evolutionary algorithm (FAEA),[23] and basin hopping[24,25] (Monte Carlo plus minimization[26]). The known global minima can be found in the Cambridge Cluster Database (CCD)[27] (for Girifalco potentials up to $N = 80$, and for PPR potentials up to $N = 105$).

Recently, we proposed a dynamic lattice searching (DLS) method and applied it to unbiased global optimization of LJ clusters.[28] All known global minima up to $N = 309$ are reproduced by DLS with a much higher efficiency than that of some other unbiased global optimization methods, for example, monotonic sequence basin-hopping (MSBH)[29] and conformational space-annealing (CSA)[30] methods. DLS can greatly reduce the number of LMs by searching the adaptively generated lattice without LM for candidates. Furthermore, DLS starts from a randomly initialized structure and utilizes a simple greedy strategy, which leads to a very high convergence speed, and various configurations may be located. Therefore,

[a] *L. Cheng, Prof. W. Cai, Prof. X. Shao*
Department of Chemistry, University of Science and Technology of China
Hefei, Anhui 230026 (P. R. China)
Fax: (+86) 551-3601592
E-mail: xshao@ustc.edu.cn

 DOI: 10.1002/cphc.200400425

DLS can be utilized for conformational analysis by counting the hit number of various configurations over a large enough number of runs.

Herein, we report on a study in which DLS was applied to the global optimization of $(C_{60})_N$ clusters up to $N=150$ using the Girifalco potential. Also, conformational analysis was carried out based on the results of 10000 independent runs. Interestingly, our calculation results are consistent with data from annealing experiments at high temperature.[7]

2. Dynamic Lattice Searching

The number of parameters is large and the searching space is continuous, so most of the best methods (such as basin hopping[24]) for cluster optimization make use of LM, for example, the limited-memory quasi-Newton method (L-BFGS).[31] Therefore, the operations of global optimization are based on local minima, and a problem with continuous searching space is turned into a combinational problem. However, LMs are very time-consuming when the cluster size N is large. Most unbiased global optimization methods are based on random mutations or random moving atoms (molecules) of the outer layer, and LMs are necessary after those operations. Therefore, the number of LMs is always very large before convergence. For example, the number of LMs needed for convergence is 1256 for LJ_{110} even if a simple greedy strategy is adopted.[29] Of course, the number will be much larger for population-based evolutionary strategies. Therefore, the key for reducing computational time is to reduce the number of LMs.

Firstly, possible locations around an unknown local minimum structure can be predicted, and all these locations are named the dynamic lattice (DL). Then the molecules with the highest potential energy are deleted from the cluster and inserted into the DL. These selected molecules are active, and the others are inert; the number of active molecules is 10–20 in this study. The potential energy of the DL sites can be calculated in advance. The number of LMs can be greatly reduced by searching the DL without LM. Based on this strategy, an efficient cluster optimization method, named dynamic lattice searching (DLS), was proposed.[28]

DLS starts from a randomly generated structure. Then, a cycle of DL construction, DL searching, and LM is performed. The DL construction procedure will adaptively generate the DL around the starting local minimum, the DL searching procedure will get some low-energy candidates, and the LM procedure will obtain the corresponding local minima of these candidates. If a better solution is located, it will be taken as the starting local minimum of the next generation. Otherwise, the current starting local minimum is taken as the result of this calculation.

DLS is somewhat similar to the seeding or modeling methods in procedure, but different in the basic theory. The seeds of DLS are randomly generated with unknown structure. In contrast to the modeling or lattice methods, the lattices in DLS are generated adaptively and, for different structures, the lattices are different too. Therefore, DLS is very fast, similar to the seeding or modeling methods, but it is entirely unbiased. Furthermore, the number of active molecules can be large as a result of the low cost and high efficiency of the DLS method. Therefore, DLS has a very high searching ability and can easily reach funnel bottoms on the PES.

3. Sequences and Global Minima

Similar to polytetrahedral clusters,[32] the Leary tetrahedron[33] is packed by tetrahedra. The difference is that the molecule number on one edge of the basic tetrahedron for the Leary tetrahedron is four. Similarly, the icosahedral and decahedral clusters can also be thought of as packed by tetrahedra. The basic tetrahedra can be strained or incomplete. Furthermore, the face-centered cubic (fcc) cluster is a fragment of a large tetrahedron. Figure 1 shows some examples of icosahedral (I), decahedral (D), Leary tetrahedral (T), and fcc (F) clusters, and the edge size (m) of the basic tetrahedron is also given. We define I(+) as I plus an antilayer (FC in ref. [34]), D(+) as D plus an antilayer (FD in ref. [34]), and F(+) as F plus a small antilayer. The antilayer does not increase the value of m. Hence, a set of sequences (mI, mI(+), mD, mD(+), mT, mF, and mF(+)) is defined. For example, the 55-molecule Mackay icosahedron is in the 3I sequence, the 38-molecule fcc cluster is in the 7F sequence, the 75-molecule Marks decahedron is in the 5D sequence, and the 98-molecule Leary tetrahedron is in the 4T sequence (Figure 1). F and T are both close-packed (cp).

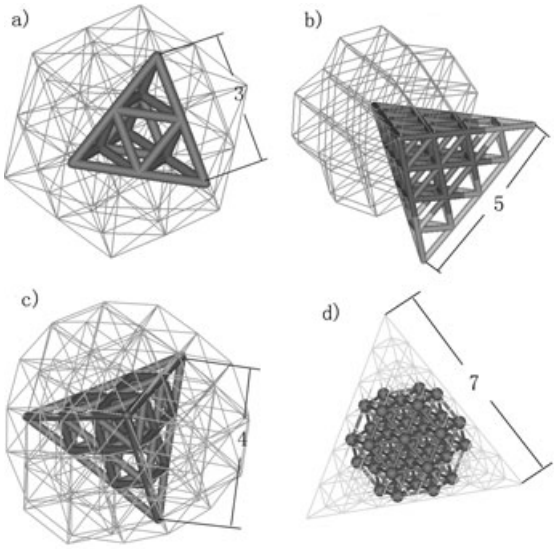

Figure 1. *Structures with various packing can be regarded as packed by basic tetrahedra: a) 55-molecule icosahedron; b) 75-molecule Marks decahedron; c) 98-molecule Leary tetrahedron; d) 38-molecule fcc cluster. The edge size of the basic tetrahedron is also marked.*

To have a sufficient study of $(C_{60})_N$ molecular clusters, DLS was applied to the clusters up to $N=150$ using the Girifalco potential based on 10000 independent runs for each case. All the known global minima given in the CCD ($N\leq 80$) are reproduced, and putative global minima up to $N=150$ are also located. The calculation was carried out on an HP cluster with

Intel Itanium 2 Madison 1.5-GHz processors. The total time consumed by the 10 000 DLS runs for all cases by using eight central processing units (CPUs) is about one week. Although the amount of time is very large, DLS is actually very fast; for example, the average CPU time per hit of global minimum of the $(C_{60})_{100}$ cluster is about 5 min. Potential energies and the sequences of the putative global minima obtained are given in Table 1 for $13 \leq N \leq 150$. Figure 2 shows the structures of some typical global minima for various sequences. The putative global minimum of $(C_{60})_{13}$ is in the 2I sequence. The putative global minimum structure of $(C_{60})_{38}$ is with perfect fcc packing and in the 7F sequence, and the global minima of $(C_{60})_{39-42}$ are all in the 7F(+) sequence. The putative global minimum of $(C_{60})_{48}$ is with decahedral packing plus an antilayer and in the 4D(+) sequence. The putative global minimum structure of $(C_{60})_{59}$ has a truncated tetrahedron core, and has antilayers on the four faces of the tetrahedron. It can be thought of as packed by five incomplete five-molecule edged tetrahedra, and the packing style is similar to that of the Leary tetrahedron. Therefore, it is defined as in the 5T sequence. Similarly, the putative global minima of $(C_{60})_{100}$ and $(C_{60})_{116}$ are in the 6T and 7T sequences, respectively. They are all unstrained and can be transformed to fcc by turning the antilayers into fcc layers. There are also some putative global minima with close packing (cp), but not in T or F(+) sequences (such as $(C_{60})_{142}$ and $(C_{60})_{149}$).

Figure 3 shows the energy of the global minima so that particularly stable clusters will stand out, and the sequences of the stable clusters are also indicated. The results presented in Figure 3 are similar to those found in ref. [12] for $N \leq 105$. Icosahedra are only lowest in energy up to $N = 13$, and decahedra are the most dominant configurations. For $N \geq 101$, most of the magic numbers in potential energy are 6D. On comparing Figure 3 with the high-temperature magic numbers observed experimentally,[7] there is some correspondence for $N = 13$, 38, 64, 71, and 75. However, there are also some contradictions when only comparing the energy, for example, for $N = 48$, 54, 58, 68, and 98. To explain this phenomenon, a sequence-based conformational analysis is carried out.

4. Sequence and Conformational Analysis

DLS starts from a randomly initialized configuration and explores better solutions around the starting configuration, thus the funnel bottom in a wider funnel on the PES will have more chances to be located. Therefore, the hit number of a configu-

Table 1. *Energies and sequences (S) for the putative global minima of $(C_{60})_N$ clusters with the Girifalco potential. cp stands for close-packed [but not for F(+) and T]. ε is the pair well depth.*

N	S	E/ε	N	S	E/ε	N	S	E/ε	N	S	E/ε
13	2I	−38.19422	48	4D(+)	−197.42965	83	cp	−372.93606	118	6D	−556.19588
14	3D	−41.96327	49	4D(+)	−201.67320	84	cp	−377.46702	119	6D	−561.45971
15	3D	−46.12082	50	cp	−207.66680	85	cp	−382.74932	120	cp	−567.18749
16	3D	−50.27908	51	cp	−211.93865	86	cp	−388.96742	121	6D	−572.92263
17	3D	−54.43807	52	cp	−217.20635	87	cp	−393.45342	122	6D	−578.30520
18	3D	−58.61860	53	cp	−221.47836	88	cp	−398.51391	123	6D	−582.67900
19	3D	−62.69319	54	5D	−226.78155	89	7T	−403.19843	124	11F(+)	−588.26419
20	3D	−66.76531	55	5D	−231.07316	90	7T	−408.48626	125	7T	−593.87840
21	3D	−70.94720	56	5D	−236.31745	91	6T	−414.78707	126	6D	−599.43738
22	3D(+)	−75.10984	57	5D	−241.56727	92	6T	−419.02258	127	6D	−603.83666
23	3D(+)	−79.94459	58	4T	−246.29744	93	cp	−424.29729	128	11F(+)	−609.36823
24	cp	−84.15632	59	5T	−252.34541	94	cp	−429.58114	129	6D	−614.36181
25	3D(+)	−88.65488	60	5T	−256.54382	95	6D	−435.25097	130	6D	−620.56945
26	cp	−93.64506	61	8F	−261.61957	96	6D	−439.64423	131	6D	−625.93052
27	cp	−97.79501	62	5T	−265.93257	97	6D	−445.12137	132	11F	−630.46268
28	3D(+)	−102.00457	63	5D	−271.27774	98	6T	−450.80553	133	6D	−635.52924
29	4D	−106.76009	64	5D	−277.44388	99	6D	−456.48250	134	7T	−641.57421
30	4D	−111.01253	65	5D	−281.76524	100	6T	−462.47150	135	6D	−647.06070
31	4D	−116.18632	66	5D	−286.97355	101	6D	−468.14156	136	11F	−651.56821
32	4D	−120.40840	67	5D	−292.19006	102	6D	−472.53236	137	cp	−657.04688
33	4D	−125.64079	68	8F(+)	−296.74668	103	6D	−477.78639	138	cp	−661.97084
34	4D	−129.85597	69	5D	−301.72964	104	6D	−483.04604	139	6D	−668.19136
35	4D	−135.08309	70	5D	−307.08892	105	6D	−487.43349	140	6D	−673.52303
36	4D	−139.28793	71	5D	−313.26322	106	6D	−492.68505	141	cp	−678.35133
37	4D	−144.50652	72	5D	−317.52213	107	6D	−497.94228	142	6D	−683.76697
38	7F	−150.57142	73	5D	−322.78073	108	6D	−504.11629	143	cp	−689.99901
39	7F	−154.73966	74	5D	−328.21873	109	6D	−508.52965	144	6D	−694.71108
40	7F	−158.90827	75	5D	−334.39505	110	6D	−513.79794	145	6D	−700.01089
41	7F(+)	−163.30689	76	5D	−338.63307	111	6D	−519.07223	146	6D	−706.32072
42	7F(+)	−167.54706	77	5D	−343.87696	112	6D	−525.25152	147	cp	−711.09825
43	cp	−172.72057	78	5D	−348.11241	113	6D	−530.65554	148	6D	−715.81139
44	cp	−176.98163	79	cp	−353.84742	114	6D	−535.03806	149	cp	−721.28425
45	cp	−182.23770	80	cp	−358.12173	115	6D	−540.28593	150	7D	−726.31754
46	cp	−186.57956	81	cp	−363.39167	116	7T	−546.18650			
47	cp	−191.67458	82	5D	−367.95573	117	6D	−551.78912			

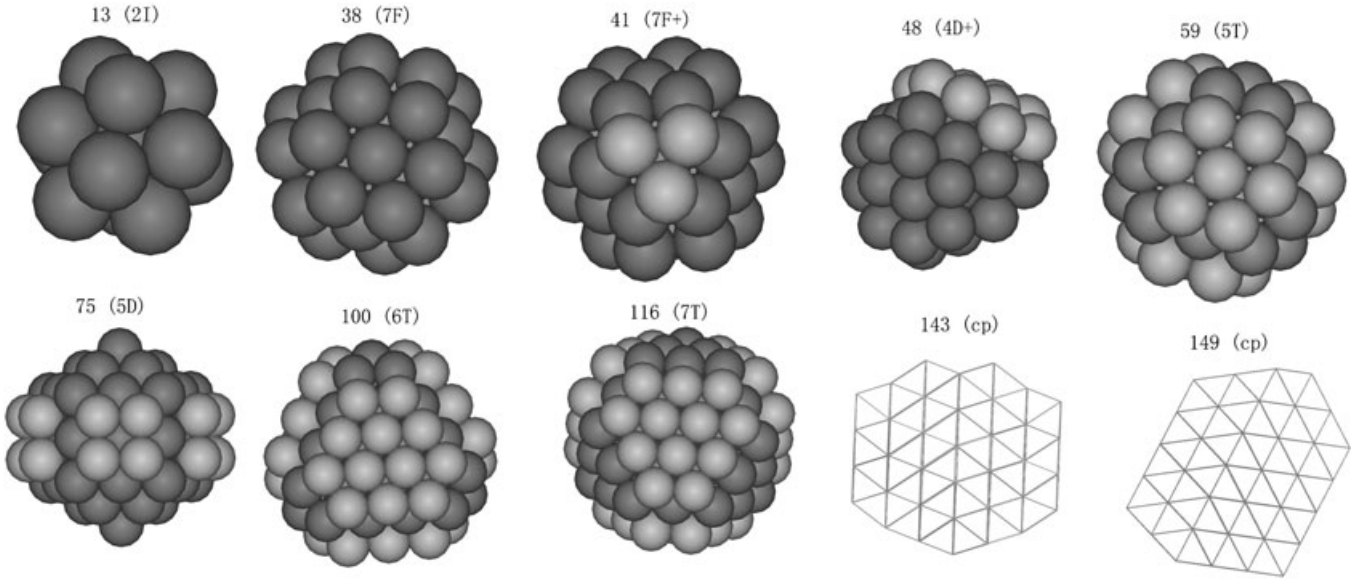

Figure 2. *Some typical global minima in various sequences.*

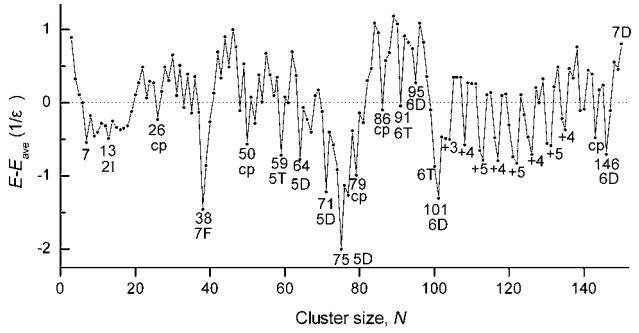

Figure 3. *Energy of the global minima for $(C_{60})_N$ clusters with the Girifalco potential. The energy zero is taken to be E_{ave}, a four-parameter fit to the energy of the global minima: $E_{ave} = -6.39171N + 7.69125N^{2/3} + 3.93111N^{1/3} - 6.3844$.*

ration over a large enough number of runs will be consistent with the width of the funnel containing the configuration. Here, the hit numbers of various funnel bottoms are recorded.

Figure 4 shows the hit number of the putative global minima over 10000 independent DLS runs, and sequence information is also presented. The dominant sequences are changed from 2I to 3D(+), 4D(+), 5D(+), and 6D(+) with increasing *N*. Other sequences are lowest in energy at the crossover of two D(+) sequences or at their magic numbers. It can be seen that the hit number of the 2I sequence is extremely large, while the number for F(+) sequences is very small; for example, for 11F ($N = 132$, 136), the hit number is only one over 10000 runs. Interestingly, there are obvious down steps of hit number from 2I to 3D(+), 4D(+), 5D(+), and 6D(+). It can be seen from the figure that a smaller *m* value generally corresponds to a larger hit number. The reason may be that a smaller *m* value corresponds to a larger number of basic tetrahedra, which leads to higher entropy. Generally, the relationship of *m* value for same cluster size is: F(+) > cp > D(+) > T > I. This may be the reason why the I sequence is most favored, while F(+) is much more difficult to locate regardless of the potential energy. It can also be seen that the hit number of structures with an antilayer is generally larger, as the antilayer can decrease the symmetry and increase the entropy. Furthermore, a small *m* value can make the clusters spherical more easily, but also more strained. Only at magic numbers can structures with a larger *m* value, such as F(+) and cp, be sufficiently spherical.

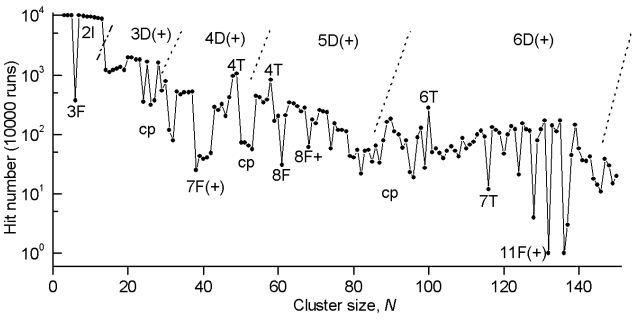

Figure 4. *The hit number of the global minima over 10000 independent runs for each case. Sequence information is also shown.*

The *m*D(+) sequences were studied to find out the magic numbers with decahedral packing. Figure 4 shows an overview of the hit number of *m*D(+) sequences. It can be seen that the hit number clearly decreases with *m* value, and does not show an evident decreasing trend with *N* within the same *m* value. This finding indicates that the search ability of DLS does not decrease with *N* for cluster size $N \leq 150$. The energy of structures in 3D(+), 4D(+), 5D(+), and 6d(+) sequences are plotted in Figure 5. The magic numbers in the figure ($N = 31$, 33, 35, 37, 39 for 4D, and $N = 54$, 64, 71, 75 for 5D) correspond very well to the results from annealing experiments[7] at 585 K. Comparison with Figure 4 reveals that the magic numbers observed in the experiments may not be magic numbers in

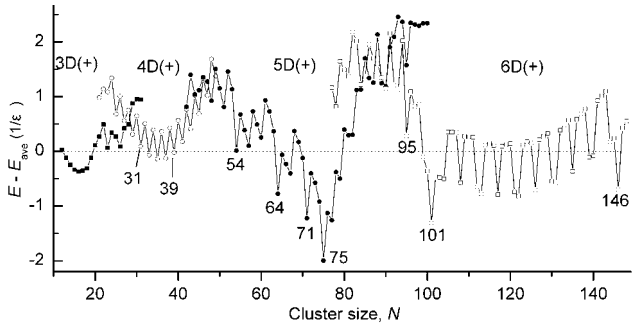

Figure 5. *Energy of the decahedral configurations for $(C_{60})_N$ clusters with the Girifalco potential. The energy zero (E_{ave}) is the fit to global minima.*

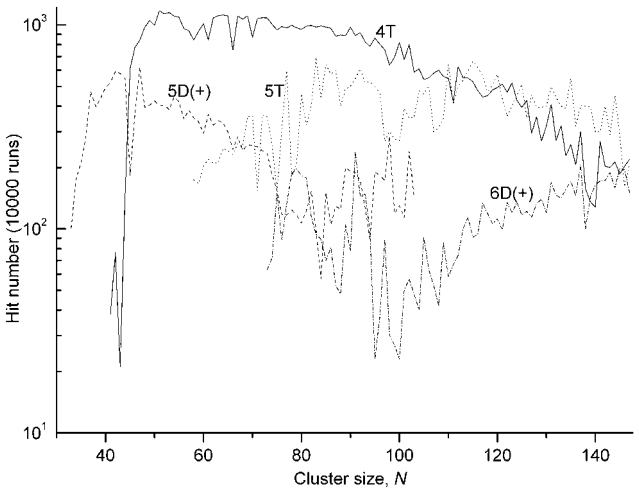

Figure 7. *Hit numbers of various sequences over 10000 independent runs.*

global minima (such as $N=54$) or may even not be global minima (such as $N=39$). This result indicates that sequences should be studied to find out the correspondence between experiments and theoretical calculations instead of only finding the global minima. Magic numbers for 6D(+) (such as $N=101$, 146) can only be observed at higher temperature (610 K) in the annealing experiments.[7] At the crossover of two D sequences, the potential energy is generally high. This may be the reason why cp structures are dominant at the crossovers (see Figure 4).

There are still some magic numbers observed in the experiments that cannot be explained. Doye[12] and Branz[7] predicted that those magic numbers are with Leary tetrahedral packing (4T in this study), by comparing the magic numbers in the 4T sequence with those observed in the experiments. Figure 6

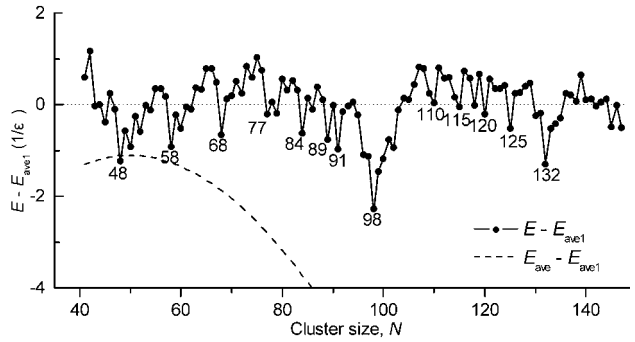

Figure 6. *Energy of the structures in the 4T sequence for $(C_{60})_N$ clusters with the Girifalco potential. The energy zero is taken to be E_{ave1}, a four-parameter fit to the energy of the 4T sequence: $E_{ave1} = -4.4849N + 9.28599N^{2/3} + 51.38782N^{1/3} - 45.03227$. (-----) is the fit to global minima.*

shows the energy of the 4T sequence. It can be seen that some magic numbers in the figure ($N=48$, 58, 68, 77, 89, 91, 98) also act as magic numbers in the experiments at high temperature, but the 4T sequence moves away from the global minima in potential energy quickly for $N \geq 50$. For example, the potential energy of the 98-molecule 4T sequence is about 3.5ε higher than that of the relative global minimum using the Girifalco potential. Interestingly, evidence for this phenomenon can be obtained by a sequence-based conformational analysis. Figure 7 shows the hit number of some selected sequences (4T, 5D(+), 5T, 6D(+)). It can be seen that 4T is the most dominant sequence in the range $45 < N < 110$. Furthermore, the hit number of 4T has very small changes for different N values, while the other sequences often have large jumps in the hit number. This phenomenon indicates that there may be large barriers between 4T and other sequences, while there may be competition within the 5D(+), 5T, 6D(+), and cp sequences. Furthermore, the unusual increasing trend for the hit rate of 6D(+) may also be caused by the competition, and this may be the reason why the peak for 101-molecule 6D is much lower than that for 146-molecule 6D. Comparison of the peak height in the experiments at high temperature with the hit rate in the DLS calculation indicates that there is also some correspondence. For example, magic numbers in the 4T sequence generally have a higher peak value in the experiments at 585 K than those in decahedral and F sequences, and this phenomenon becomes more evident at higher temperature (610 K).

The structures of some magic numbers in 4T sequences are given in Figure 8. We found some crossovers for 4T with other sequences. The 48-molecule 4T can also be thought of as 48-molecule 4D(+) (see Figure 2), but it does not act as a magic number in the 4D(+) sequence. More interestingly, the 68-molecule 4T can be regarded as a fragment of the 147-molecule Mackay icosahedron (4I). Although there are crossovers between sequences, the m value does not change for a given configuration, and the crossover may be the bridge for transitions between sequences. The configuration for the 132-molecule 4T (Figure 8) is very interesting, and can be thought of as a union of two 98-molecule 4T sequences. The 132-molecule 4T acts as a magic number in the 4T sequence, but it does not act as a magic number in the experiments. The reason may be that it is too far away from the global minima in potential energy (about 13ε higher), and its hit rate is also much lower than that for small 4T.

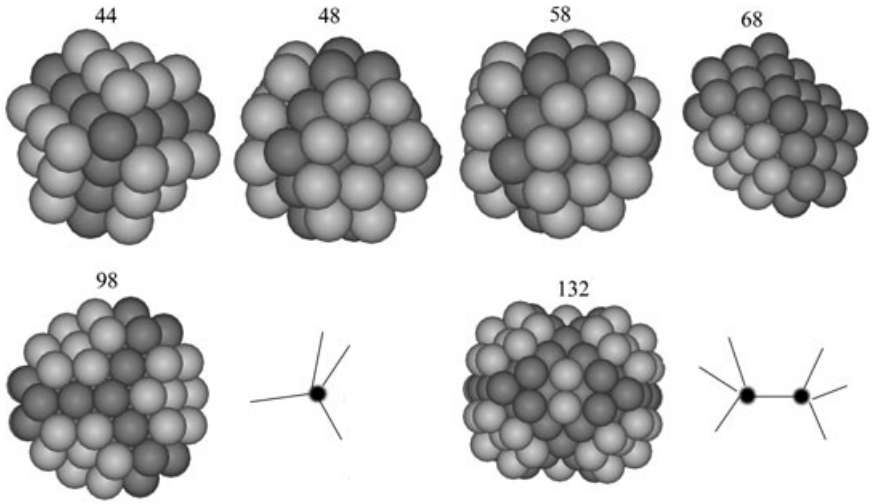

Figure 8. *Structures of some magic numbers in the 4T sequence.*

5. Conclusions

A newly proposed unbiased global optimization method, named dynamic lattice searching (DLS), has been used to locate putative global minima for the $(C_{60})_N$ clusters with Girifalco potential for all clusters up to $N=150$. As a simple greedy strategy is adopted for the basic frame, DLS has a very high convergence speed. The size of the basic tetrahedron (m) is a very important parameter, which is related to the entropy and hit number of a structure. Therefore, a new set of sequences with different m values and configurations is defined in this study. A sequence-based conformational analysis is carried out with the newly defined sequences, by counting the hit number over 10000 independent DLS runs for all cases up to $N=150$. The Leary tetrahedral sequence (4T) is proved to be dominant in a certain range of cluster sizes, although it has no potential energy advantage. Our calculation results correspond to data from the annealing experiments at high temperature, both in magic numbers and height of the peaks in the mass spectrum. Therefore, DLS may be a good tool for cluster conformational analysis.

Acknowledgements

This study is supported by the outstanding youth fund (No.20325517) from the National Natural Scientific Foundation of China (NNSFC), and the Teaching and Research Award Program for Outstanding Young Teachers (TRAPOYT) in higher education institutions of the Ministry of Education (MOE), P. R. China. Thanks to the USTC-HP High-Performance Computing Joint Lab (HPCJL) for affording the HP cluster.

Keywords: cluster compounds · conformation analysis · fullerenes · geometry optimization · sequence determination

[1] M. H. J. Hagen, E. J. Meijer, G. C. A. M. Mooij, D. Frenkel, H. N. W. Lekkerkerker, *Nature* **1993**, *365*, 425.
[2] L. Mederos, G. Navascués, *Phys. Rev. B* **1994**, *50*, 1301.
[3] J. Q. Broughton, J. V. Lill, J. K. Johnson, *Phys. Rev. B* **1997**, *55*, 2808.
[4] A. L. C. Ferreira, J. M. Pacheco, J. P. Prates-Ramalho, *J. Chem. Phys.* **2000**, *113*, 738.
[5] T. P. Martin, U. Näher, H. Schaber, U. Zimmermann, *Phys. Rev. Lett.* **1993**, *70*, 3079.
[6] W. Branz, N. Malinowski, H. Schaber, T. P. Martin, *Chem. Phys. Lett.* **2000**, *328*, 245.
[7] W. Branz, N. Malinowski, A. Enders, T. P. Martin, *Phys. Rev. B* **2002**, *66*, 94107.
[8] J. P. K. Doye, D. J. Wales, *Chem. Phys. Lett.* **1996**, *262*, 167.
[9] J. P. K. Doye, A. Dullweber, D. J. Wales, *Chem. Phys. Lett.* **1997**, *269*, 408.
[10] W. H. Zhang, L. Liu, J. Zhuang, Y. F. Li, *Phys. Rev. B* **2000**, *62*, 8276.
[11] W. S. Cai, Y. Feng, X. G. Shao, Z. X. Pan, *Chem. Phys. Lett.* **2002**, *359*, 27.
[12] J. P. K. Doye, D. J. Wales, W. Branz, F. Calvo, *Phys. Rev. B* **2001**, *64*, 235409.
[13] L. A. Girifalco, *J. Phys. Chem.* **1992**, *96*, 858.
[14] A. Cheng, M. L. Klein, *Phys. Rev. B* **1992**, *45*, 1889.
[15] J. M. Pacheco, J. P. Prates-Ramalho, *Phys. Rev. Lett.* **1997**, *79*, 3873.
[16] J. P. K. Doye, D. J. Wales, *Phys. Rev. Lett.* **1998**, *80*, 1357.
[17] C. L. Cleveland, W. D. Luedtke, U. Landman, *Phys. Rev. Lett.* **1998**, *81*, 2036.
[18] J. P. Neirotti, F. Calvo, D. L. Freeman, J. D. Doll, *J. Chem. Phys.* **2000**, *112*, 10304.
[19] J. P. K. Doye, F. Calvo, *Phys. Rev. Lett.* **2001**, *86*, 3570.
[20] F. Calvo, *J. Phys. Chem. B* **2001**, *105*, 2183.
[21] F. Baletto, J. P. K. Doye, R. Ferrando, *Phys. Rev. Lett.* **2002**, *88*, 75503.
[22] J. P. K. Doye, M. A. Miller, D. J. Wales, *J. Chem. Phys.* **1999**, *111*, 8417.
[23] W. S. Cai, X. G. Shao, *J. Comput. Chem.* **2002**, *23*, 427.
[24] D. J. Wales, J. P. K. Doye, *J. Phys. Chem. A* **1997**, *101*, 5111.
[25] D. J. Wales, H. A. Scherage, *Science* **1999**, *285*, 1368.
[26] Z. Li, H. A. Scheraga, *Proc. Natl. Acad. Sci. U. S. A.* **1987**, *84*, 6611.
[27] The Cambridge Cluster Database, available at http://www-wales.ch.cam.ac.uk/CCD.html.
[28] X. G. Shao, L. J. Cheng, W. S. Cai, *J. Comput. Chem.* **2004**, *25*, 1693.
[29] R. H. Leary, *J. Global Optim.* **2000**, *18*, 367.
[30] J. Lee, I. H. Lee, J. Lee, *Phys. Rev. Lett.* **2003**, *91*, 80201.
[31] D. C. Liu, J. Nocedal, *Math. Program.* **1989**, *45*, 503.
[32] J. P. K. Doye, D. J. Wales, *Phys. Rev. Lett.* **2001**, *86*, 5719.
[33] R. H. Leary, J. P. K. Doye, *Phys. Rev. E* **1999**, *60*, R6320.
[34] D. Romero, C. Barrón, S. Gómez, *Comput. Phys. Commun.* **1999**, *123*, 87.

Received: September 7, 2004

